PCCP

ARTICLE

Nonlinear imaging microscopy for assessing structural and photochemical modifications upon laser removal of dammar varnish on photosensitive substrates

Received 00th January 20xx,
Accepted 00th January 20xx

DOI: 10.1039/x0xx00000x

www.rsc.org/

M. Oujja[a], S. Psilodimitrakopoulos[b], E. Carrasco[a,c], M. Sanz[a], A. Philippidis[b], A. Selimis[b], P. Pouli[b], G. Filippidis[b], M. Castillejo[a]†

The nonlinear optical microscopy (NLM) modalities of Multi-Photon Excited Fluorescence (MPEF) and Third Harmonic Generation (THG) have been combined in this work to characterize as a function of depth with micrometric resolution the type and extent of morphological and photochemical modifications that take place upon ultraviolet (UV) pulsed laser removal of a dammar varnish layer applied on a photosensitive substrate. The latter consist on a layer of the synthetic polymer poly-methyl methacrylate doped with a photosensitizer, the aromatic compound 1,4-di[2-(5-phenyloxazolyl)] benzene, that strongly fluoresces upon UV light illumination. A number of laser conditions for partial or total elimination of the varnish coating were explored, namely different wavelengths (266, 248 and 213 nm) and pulse durations, in the nanosecond, picosecond and femtosecond ranges. Changes in the MPEF signals upon laser ablation of the outermost varnish layer successfully signpost photochemical modifications of the varnish or of the photosensitive under-layer, and their dependence with the laser ablation parameters, i.e., wavelength and pulse duration. In turn, THG signals mark the presence of layer boundaries and the reduction by laser ablation of the thickness of the varnish coating. The obtained MPEF and THG data are complemented by morphological observation by optical microscopy and measurements of laser induced fluorescence and micro-Raman spectra of the samples before and after laser ablation at the selected laser irradiation conditions. The results acquired through these non-destructive NLM imaging techniques serve to understand the phenomena that are induced upon laser ablation and to determine the best operating conditions that ensure controlled removal of the varnish with minimal morphological and chemical modifications to the under-layers. This research is of direct application to the UV pulsed laser cleaning of paintings and demonstrates the potential of NLM as a novel assessment tool for non-destructive, on line monitoring of the laser cleaning process.

1. Introduction

In the restoration of paintings, the removal of the superficial, deteriorated varnish without affecting the underlying paint layer constitutes a delicate intervention, in many cases necessary to rectify the optical and aesthetic properties of the painted surface and to extend the lifetime of the artwork [1,2]. Laser-assisted removal of degraded varnish coatings takes advantage of the high spatial resolution, accuracy, material selectivity and immediate feedback associated with the process of laser ablation [3] and, thus, it can be particularly advantageous in comparison to a number of conventional cleaning methodologies used in the field. Accurate control in the elimination of the varnish layer can be achieved by using ultraviolet (UV) pulsed lasers to ensure strong light absorption by the varnish and consequently the light confinement to the top, most aged, polymerized layer [4,5 and references therein]. Under this condition, the laser light transmitted to the underlying painting is negligible and undesired harm to light-sensitive painting materials (pigments, binders) can be avoided [4-7]. Research on laser cleaning of paintings helps to develop strategies to circumvent the possible side effects. To that respect, several studies, using model and real samples, have concentrated on identifying, according to the degradation state of the varnishes and the substrate materials, the most adequate laser conditions and irradiation protocols, by selection of wavelength, pulse duration, spatial profile, fluence values, number of pulses, etc. [8-13]. In parallel, the assessment of the structural and photochemical modifications [14-16] that could be induced on the irradiated multi-layered substrates as a result of laser ablation is crucial to develop advanced, safe laser cleaning methodologies in the restoration of paintings.

Imaging based on nonlinear optical microscopy (NLM), a technique initially developed in the field of biomedical optics [17, 18], allows surface mapping and profiling of multi-layer structures and, more recently, it is being increasingly applied to examine substrates of interest in cultural heritage [19-24]. NLM imaging relies on near infrared (IR), ultrafast laser excitation (pulse duration in the range of femtoseconds) to exploit several nonlinear optical effects that allow high contrast imaging of samples. In particular, the NLM imaging modalities of Multi-Photon Excited Fluorescence (MPEF), Second and Third Harmonic Generation (SHG, THG) provide non-destructive accurate determination of the chemical nature, structure and thickness within multi-layered samples. MPEF relies on the measurement of the intrinsic fluorescence from materials, a property related to their chemical composition. SHG signals are only produced by non-centrosymmetric media and yield information on

[a] Instituto de Química Física Rocasolano, IQFR-CSIC, Serrano 119, 28006 Madrid, Spain.
[b] Institute of Electronic Structure and Laser (IESL), Foundation for Research and Technology -Hellas (FORTH), P.O. Box 1385, 71110, Heraklion, Crete, Greece.
[c] Present address: IMDEA Nanociencia, 28049 Madrid, Spain.
† Email: marta.castillejo@iqfr.csic.es.

the presence of crystalline materials or of hierarchical and highly oriented structures without inversion symmetry. Finally, THG marks the local differences of third-order nonlinear susceptibilities, refractive index and dispersion, and serves to localize the position of interfaces between optically dissimilar media in multi-component, multi-layer samples.

NLM imaging has been applied before for the assessment of painting substrates and painting mock-ups [20, 25, 26]. In particular, Filippidis *et al.* [26] have demonstrated the capacities of the technique to assess the in-depth degradation of varnishes due to ageing. In this study the NLM imaging modalities of MPEF and THG have been employed to systematically characterize with micrometric resolution the type and extent of the in-depth morphological and photochemical modifications that could be induced on the underlying painting layers upon ultraviolet (UV) laser removal of a varnish protective coating.

Methodologies based on the use of model probes for evaluating in-depth modifications induced by UV laser ablation of polymeric materials have been applied in previous works [3, 16, 25, 27]. This study is conducted in model samples that represent realistic models of a varnished painting. The samples are constituted by bi-layers, where the top varnish layer coats a doped synthetic polymer film, the latter playing the role a painted substrate. The dopant is a photosensitive dye that strongly fluoresces upon UV light illumination and upon multiphoton absorption of the excitation near IR, femtosecond laser. performed in samples. This approach serves the purpose of identifying the fundamental physicochemical processes induced by laser ablation, both on the varnish and in the underlying photosensitive substrate. A number of laser conditions for partial or total elimination of the varnish coating have been explored, namely three different UV wavelengths (266, 248 and 213 nm) and pulse durations in the nanosecond (ns), picosecond (ps) and femtosecond (fs) ranges. The obtained MPEF and THG NLM data are complemented by morphological observations by optical microscopy (OM) and measurements of laser induced fluorescence (LIF) and micro-Raman spectra of the samples before and after laser ablation at the selected laser irradiation conditions.

In this work, the detailed analysis of the information obtained by NLM imaging serves to address and evaluate the induced structural and photochemical modifications, with micrometric resolution both in surface and in depth, that take place in the polymer coating and in the photosensitive underlying substrate during laser ablation of the outer polymeric coating and helps to determine the best operating conditions that ensure controlled removal of the varnish with minimal morphological and chemical modifications to the under-layers. Therefore, this research allows establishing NLM imaging as a powerful non-destructive diagnostic tool with significant potential in the field of painting restoration.

2. Experimental

2.1. Samples

The prepared model samples aim to simulate the real case of a painting layer, where a pigment is dispersed in a binding medium coated by a varnish film. The samples (Fig. 1) are constituted by bi-layers: a top layer of dammar, a triterpenoid varnish commonly used in paintings, and an under-lying layer that simulates the paint layer and is made of a doped synthetic polymer film. We used poly-methyl methacrylate (PMMA, MW~ 996 kDa) doped with a photosensitizer, the aromatic compound 1,4-di[2-(5-phenyloxazolyl)] benzene (POPOP). PMMA was chosen due to its negligible fluorescence upon single UV photon and multiphoton absorption of the NLM, near IR femtosecond exciting laser. The selection of POPOP is motivated by the high transparency of this compound at the excitation wavelength of 1028 nm and by its strong fluorescence emission, centred in the region of 410 nm, which can be induced by multiphoton absorption of the near IR laser [28]. Dammar is also transparent at 1028 nm and yields fluorescence emission at 435 nm [29] upon multiphoton excitation at this wavelength. Therefore, the selection of the present combination of materials, ensures the possibility of evaluating the MPEF signals and, through the combination with THG measurements (see below), of analysing the ablating laser induced morphological and photochemical modifications of the involved layers.

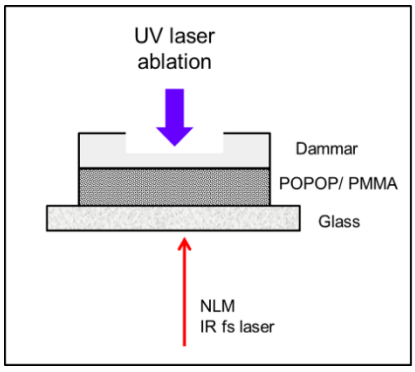

Fig. 1. Scheme of bi-layer samples constituted by a dammar coated POPOP/PMMA film deposited on a glass plate. For NLM measurements the samples are positioned as to expose the glass plate to the near IR femtosecond laser pulses.

The films were prepared by casting solutions of POPOP/PMMA in dichloromethane (CH_2Cl_2) on thin glass plates (75 μm thick) and were subsequently air-dried. The dopant (POPOP) concentration was 0.5 w/w % and the film thickness was in the range of 10–20 μm, as measured by profilometry. A layer of dammar varnish (from a solution in tetrachloroethylene, C_2Cl_4, 18 w/v %) was casted over the doped polymer film and again was air-dried in a fume hood. The thickness of the varnish film varied from 150 to 250 μm. For the purpose of this study, and in contrast to the real cases/scenarios, it was chosen to have the top varnish layer significantly thicker in comparison to the lower layer (doped PMMA simulating the painting) in order to be able to experiment various levels of varnish removal, as well as to investigate rather extreme laser ablation conditions (i.e., high number of pulses).

The absorption spectrum of a thin (about 2 μm) dammar film casted on quartz was measured using a UV-Vis Spectrometer (Perkin Elmer-Lambda 950, Waltham, Massachusetts, USA) and is shown in Figure 2. In agreement with previously reported data [1, 29], and despite the fact that the samples studied here are not aged, the spectrum shows the differences of absorption of the varnish in the UV and in

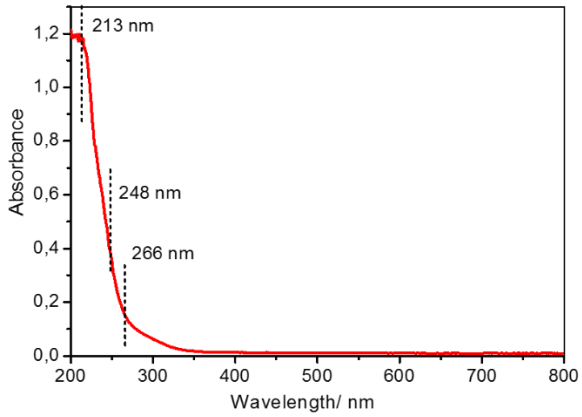

Fig. 2. UV-Vis absorption spectrum of a 2 μm thick dammar–layer on quartz. The wavelengths used for laser ablation are indicated by vertical dotted lines.

Table 1. Laser systems used for ablation of the top dammar coating in bi-layer samples (Fig. 1) and corresponding operating conditions.

Laser system	Wavelength (nm)	Pulse duration	Spatial profile	Rep. rate (Hz)	Fluence (mJ/cm^2)
Nd:YAG, B.M. Industries, 5000	266, (4th harmonic)	8 ns	Gaussian-like	3.33	800, 1270
Nd:YAG, Lotis II, LS-2147	213, (5th harmonic)	15 ns	Gaussian-like	2	120, 269
Nd:YAG, EKSPLA, SL-312	266, 213 (4th, 5th harmonics)	150 ps	Gaussian-like	3.33	At 266 nm: 310, 685 At 213 nm: 130, 270
fs KrF excimer-dye laser system	248	500 fs	Top hat	3	310, 685

the visible-to-IR regions. In the figure, the wavelengths of 213, 248 and 266 nm used for laser ablation of the dammar coating are marked as discontinuous vertical lines. In this UV region, the absorbance of the film decreases as the laser ablation wavelength increases. At the wavelength of the IR, femtosecond laser excitation beam used for NLM analysis (1028 nm), the absorption of dammar is negligible (not shown).

2.2. Laser ablation for varnish removal.

The samples were subjected to UV laser irradiation in order to remove part or the whole dammar layer by ablation using various combinations of fluence values and/or number of applied pulses.

Different laser sources, emitting at the three UV wavelengths of 266, 248 and 213 nm and delivering pulses of ns, ps and fs duration, were employed. These are three Nd:YAG systems operating at their 4th or 5th harmonics with pulses of 8, 15 ns or 150 ps and a femtosecond KrF excimer-dye laser system operating on the principle of distributed feedback emitting pulses of 500 fs at 248 nm. Table 1 lists the main characteristics of the laser ablation systems employed and the fluence values applied for ablation of the varnish. For each wavelength and pulse duration, laser irradiated areas, with a typical diameter/ length of 300 μm, were created by applying two different fluence values, approximately equivalent to two and four times the corresponding laser ablation thresholds [13, 29]. The applied number of pulses varied according to the fluence value and the desired cleaning level (partial or total varnish removal) of the studied samples.

2.3. Nonlinear microscopy imaging

The extent and in-depth dimensions of the modifications induced by partial or total removal of the dammar varnish film on the underlying layers were investigated by measuring the nonlinear MPEF and THG signals using a tightly focused IR, femtosecond laser as excitation source that propagates through the sample with incidence on its glass side (Fig. 1). Both types of signals, generated simultaneously within the focal volume at the sample plane, were obtained with an experimental set-up that has been described in detail in previous publications [26]. It is based in a custom made upright nonlinear microscope and a linearly polarized laser (Amplitude Systems, Pessac, France) operating at 1028 nm and delivering 200 fs pulses at a repetition rate of 50 MHz, with an average power of 1 W. A high numerical aperture (NA 0.8, air immersion) objective lens is employed to achieve tight focusing of the laser beam onto the sample. The power applied on the samples is of 40 mW. The focal plane within the sample was selected with a 1 μm resolution motorized translation stage. High resolution images were obtained by scanning with a pair of galvanometric mirrors and using a LabView interface to control scanning and data acquisition. MPEF signals were collected in the reflection mode using a photomultiplier tube (PMT). To cut off the reflected laser light, a short pass filter (SPF 700 nm) was placed in front of the PMT. THG signals were detected simultaneously in transmission mode through a coloured glass filter (U340 nm, Hoya, Cambridge, England) with a second PMT. Nonlinear measurement of a single spot typically lasts few seconds while a cross-sectional scanning takes less than 2 min. The lateral and axial resolution of this experimental set-up is ~ 750 nm and ~ 2 μm respectively. The vertical distortion, induced by the refractive index change between the different materials (air, dammar, POPOP/PMMA) as the laser radiation is focused within the sample volume, is taken into account. So, for all the NLM measurements, correction for apparent depth distortion is performed [30].

2.4. Complementary techniques: Optical microscopy, Laser Induced Fluorescence and micro-Raman spectroscopy

Optical Microscopy (OM) images of the dammar surface of the samples were acquired before and after laser ablation with an optical microscope (Nikon Eclipse ME600 microscope, 20X, NA of 0.46) equipped with a CCD camera. Single photon Laser Induced Fluorescence (LIF) was employed to obtain complementary chemical information from the initial and laser irradiated varnish surface of the samples. In this case, fluorescence was induced by excitation under normal incidence at 248 nm with the KrF excimer pumped dye laser system (see Table 1) using a very low fluence value, of about 1 mJ/cm^2. The fluorescence emission was collected by an optical fibre,

placed 2 cm away from the surface of the sample and nearly perpendicular to it, and spectrally analysed in a 0.30 m grating spectrograph. The spectrum was recorded on an ICCD camera (intensified charge- coupled device, Andor Solis, ICCD3759). Proper cut-off filters were employed to block scattered light from the excitation laser beam.

Further chemical information from the surface of the varnish layers was gathered with a mobile Raman Spectrometer (HE 785, Horiba Jobin Yvon) based on a 785 nm diode laser source [26]. The laser is coupled by an optical fiber to a compact probe head containing the necessary optics for sample excitation and signal collection. The backscattered light is delivered to a concave fixed grating spectrograph and a Peltier-cooled CCD detector (Horiba Synapse, Lille, France). An edge-filter in front of the spectrometer rejects the Rayleigh scattering while allowing Raman shifted emission to pass through. Spectra were acquired with the following parameters: 4 cm^{-1} resolution using a 20X objective lens, spot size of analysis in the order of 15 μm, 25 mW laser power, 60 s typical integration time while the number of accumulated scans for this study was 5.

3. Results and discussion

The samples were measured by applying the MPEF and THG modalities of NLM before and after laser ablation under several irradiation conditions, as listed in Table 1. Figure 3 shows the bimodal nonlinear images of a sample before irradiation (a), and after partial or total removal by laser ablation of the top dammar layer at 266 nm using (b) 115, (c) 346 and (d) 692 pulses of 150 ps with a fluence, F= 310 mJ/cm^2 (equivalent to twice the ablation threshold for pulses of this wavelength). In Figs. 3e and 3f, representative plots of the pixel brightness distribution across a vertical line of the images are displayed. In these plots the intensities of the THG and MPEF signals are normalized to the value obtained at the corresponding non-irradiated spot.

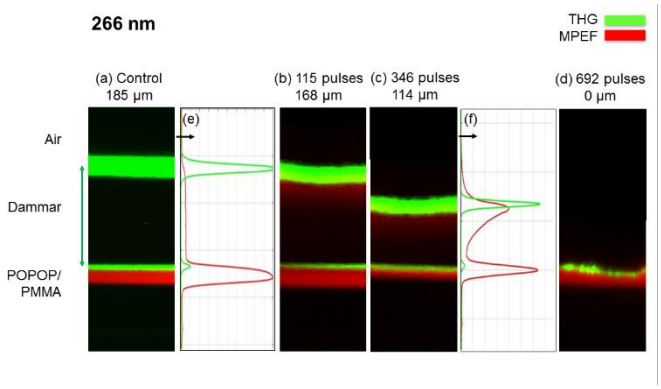

Fig. 3. Cross sectional multimodal nonlinear imaging of a POPOP/PMMA sample coated with dammar upon irradiation at 266 nm, 150 ps with F= 310 mJ/cm^2 and the indicated number of pulses: (a) 0, non-irradiated, (b) 115, (c) 346 and (d) 692. The red and green colours correspond to MPEF and THG signals respectively. Green double arrows indicate dammar thickness. The thicknesses of the initial and the remaining dammar layer are also given. The horizontal dimension of the images is 100 μm. Representative plots of the pixel brightness distribution (e) and (f) are displayed next to the corresponding nonlinear images. The intensities of the MPEF and THG signals are normalized to the value obtained at the corresponding control region (close to the ablated spot).

The green fringes in Figs. 3a to 3d and the green lines in Figs. 3e and 3f correspond to the THG signals that mark the two interfaces between the three layers, i.e. air-dammar and dammar-POPOP/PMMA. The vertical displacement of the position of the air-dammar interface reveals the gradual thickness reduction of the varnish layer with the number of the applied ablating pulses, from the initial value of 185 μm (Fig. 3a) to its total elimination after 692 pulses (Fig. 3d). It is appreciated that the THG response from the air-dammar interface is more intense than that of the dammar-POPOP/PMMA interface and that the in-depth dimension is larger for the former (Fig. 3e). These differences can be understood by taking into account that the air-dammar interface is closer to the detector that measures the THG signal in transmission mode. Moreover, the THG signals, at 343 nm, generated from the dammar-POPOP/PMMA interface are reabsorbed by the layer of dammar. Finally, it is also observed that the intensity of the THG signal from the air-dammar interface decreases upon ablation of the outer dammar coating, possibly due to the fact that the generated third harmonic of the near IR femtosecond laser has to propagate through the superficial dammar region, morphologically affected by ablation at the low absorbing wavelength of 266 nm (see OM images below).

On the other hand, the areas and lines coloured in red in Fig. 3 signpost the sample regions with MPEF response. In Figs. 3a to 3d, the red fringes below the dammar-POPOP/PMMA interface are due to POPOP fluorescence. The MPEF signal from the dammar layer is, before ablation, very weak and constant with depth (Figs. 3a, 3e) but, as ablation proceeds with an increasing number of pulses, a noticeable emission is observed, with maximum value close to the interface with air and decreasing with depth. This is clearly shown in both the images (Figs. 3b and 3c) and the pixel brightness distribution plot (Fig. 3f). The increased dammar fluorescence is attributed to oxidative degradation of dammar [29, 31], following exposure to the transmitted, UV ablating laser light. The dammar layer is affected by the 266 nm laser light up to a depth that is considerably larger than the mean penetration depth, estimated in a value of around 12 μm [29]. This result gives a clear indication of the capacity of the NLM technique to evaluate the real extent of the photochemical changes induced by laser ablation at a weakly absorbed wavelength.

Additionally, the MPEF measurements give evidence of the quenching of the signal from POPOP upon increased removal of the protecting dammar coating by ablation (Fig. 3f). In fact, UV ablation reduces the dammar thickness layer resulting in larger UV light transmission and, consequently, in higher probability of photochemical alteration or photobleaching of the POPOP fluorophore, that results in fading of its fluorescence emission upon IR multiphoton excitation from the femtosecond laser. Taking into account the mean penetration depth noted above, it is possible to estimate the photon intensity that reaches the doped polymer layer for each laser ablation pulse of 266 nm, 150 ps. Assuming an approximately 100 μm thick varnish layer, the estimation yields a value of around 10 W/cm^2, high enough to justify the observed reduction of fluorophore emission [32].

The results shown in Fig. 3 exemplify the case of ablation at 266 nm with 150 ps pulses. However similar results were obtained upon

ablation of the dammar layer with pulses of 8 ns of the same wavelength (not shown). This provides an indication of the decisive role of the light absorption properties of the varnish on the changes taking place upon ablation in the studied bi-layer samples.

The samples were also subjected to ablation with pulses of 500 fs at 248 nm, where absorption of dammar is somewhat higher than that at 266 nm (Fig. 2). Representative NLM results upon ablation with a fluence F= 685 mJ/cm^2 (equivalent to four times the ablation threshold at this wavelength) are shown in Fig. 4. Due to the THG response of the interfaces, it is observed that the dammar layer thickness decreases from an initial value of 159 μm to 55 μm after applying 80 pulses. Again, as noticed for ablation at 266 nm, the THG signal from the air-dammar interface is more intense than that of the dammar-POPOP/PMMA interface (Figs. 4a, 4d) due to the closer distance of the former to the detector and to partial absorption by the dammar layer. At this wavelength of 248 nm, and in similarity with the observation at 266 nm, the intensity of the THG signal from the air-dammar interface also decreases upon ablation of the dammar coating, although the effect is less noticeable (Figs. 4b and 4e). The difference suggests a lower degree of morphological modification of the dammar surface at a shorter, more strongly absorbed ablating laser wavelength (as confirmed by OM, see below). At 248 nm, the MPEF results are in contrast with observations upon ablation at 266 nm, as the intrinsically weak varnish fluorescence is only slightly affected by ablation of the upper layer.

However, as for ablation at 266 nm, the MPEF signal intensity from POPOP also decreases, in this case as a result of photobleaching by transmitted UV photons reaching the doped polymer layer. The estimation of the photon intensity for each laser ablation pulse of 248 nm, 500 fs, transmitted to this layer yields a value high enough to explain the fading of POPOP fluorescence under the given irradiation conditions.

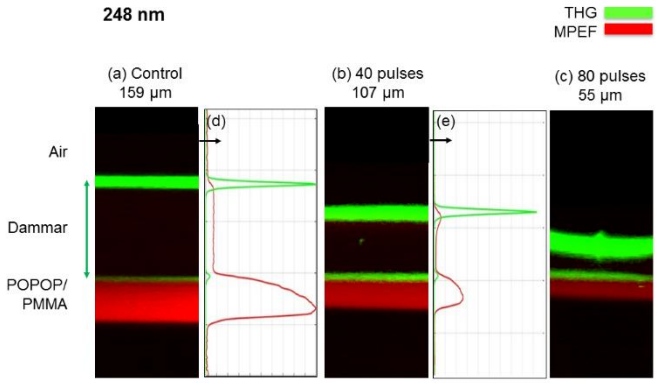

Fig. 4. Cross sectional multimodal nonlinear imaging of a POPOP/PMMA sample coated with dammar: upon irradiation at 248 nm, 500 fs with F= 685 mJ/cm^2 at the indicated number of pulses: (a) 0, non-irradiated, (b) 40 and (c) 80. The red and green colours correspond to MPEF and THG signals respectively. Green double arrows indicate dammar thickness. The thicknesses of the initial and the remaining dammar layer are also given. The horizontal dimension of the images is 100 μm. Representative plots of the pixel brightness distribution (d) and (e) are displayed next the corresponding nonlinear images. The intensities of the MPEF and THG signals are normalized to the value obtained at the corresponding control region (close to the ablated spot).

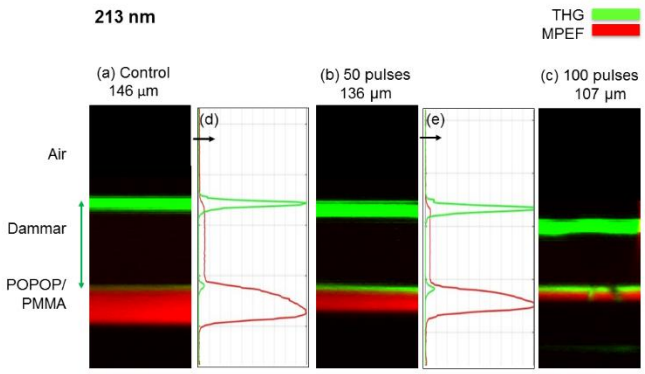

Fig. 5. Cross sectional multimodal nonlinear imaging of a POPOP/PMMA sample coated with dammar: upon irradiation at 213 nm, 150ps with F= 269 mJ/cm^2 at the indicated number of pulses: (a) 0, non-irradiated, (b) 50, (c) 100. The red and green colours correspond to MPEF and THG signals respectively. Green double arrows indicate dammar thickness. The thicknesses of the initial and the remaining dammar layer are also given. The horizontal dimension of the images is 100 μm. Representative plots of the pixel brightness distribution (d) and (e) are displayed next to the corresponding nonlinear images. The intensities of the MPEF and THG signals are normalized to the value obtained at the corresponding control region (close to the ablated spot).

The main NLM results obtained upon ablation at 213 nm, a wavelength where transmission to the under-layer should be highly reduced (Fig. 2), are displayed in Fig. 5. These correspond to ablation with 150 ps pulses at a fluence F= 269 mJ/cm^2 (equivalent to four times the ablation threshold with pulses of this wavelength). Under these conditions, the NLM signals reveal that fluorescence from dammar and the POPOP/PMMA layer remains unaltered upon ablation. The highly absorbed, ablating UV photons are effective in thinning down the dammar layer without modifying the fluorescence properties of the bi-layer components, due to the negligible UV light transmission. As mentioned for the case of 266 nm, here again the differences observed by NLM imaging upon ablation with 150 ps and 15 ns are negligible.

To better understand the results obtained through NLM imaging, we acquired complementary OM images and LIF and Raman spectra of the non-irradiated (control) and laser ablated samples. Fig. 6 displays OM images of the surface of laser ablation spots at the three wavelengths of this study. Formation of bubbles, with characteristic micrometre sizes, is clearly appreciated upon ablation at 266 nm (Fig. 6 a), while less morphological alterations, with signs of melting phenomena, were recorded upon irradiation at 248 nm (Fig. 6b). In contrast, at 213 nm the edge delimiting the ablated area marks the flat, smooth surface left after ablation of dammar at this wavelength (Fig. 6c, left part). Although the morphology of irradiated areas of the unaged samples of this study may differ to a certain extent from that reported from aged dammar samples [13, 29], the morphological aspect of the surfaces shown herein support the evidence that ablation at the weakly absorbed wavelength of 266 nm induces a change of the superficial morphology of the fresh dammar surface. This effect is noticeable, but in lesser extent, at 248 nm while, on the contrary, the surface of the dammar varnish ablated at 213 nm remains morphologically unaffected. The different superficial morphologies influence the propagation of the THG collected in transmission mode (Fig. 1) and partly explain the

reduction of the signal from the air-dammar interface upon ablation of the outer dammar coating at 266 and 248 nm (as observed in Figs. 3f and 4e).

The MPEF results shown above are based in the intrinsic fluorescence signals of the materials used in the bi-layer samples. The single- and multiphoton laser induced florescence of dammar has been thoroughly studied [26, 29]. In terms of photon energy, three and four photon absorption of the femtosecond, 1028 nm laser are equivalent to single photon absorption at 342 and 257 nm respectively. To verify the origin of the MPEF signals, LIF spectra were acquired by excitation of the dammar surface at 248 nm. Before ablation (Figs. 7a, b, black lines) the spectra consist of a broad band with maximum emission at 435 nm. This is in agreement with reported literature results, acquired over a range of UV excitation wavelengths and various degrees of aging of the varnish [13, 20, 26, 29, 31]. Partial laser ablation of the dammar layer at 266 nm (Fig. 7a, red line), appreciably increases the LIF intensity without spectral band modification. Correspondingly, it should be expected that the observed increase of MPEF signal from dammar at the poorly absorbed wavelength of 266 nm (Figs. 3b, 3c, 3f) is due to a larger fluorescence yield of the varnish induced by ablation and not to a spectral band modification. Differently, the LIF spectrum from dammar remains unaltered, both in intensity and shape, after ablation at 213 nm (Fig. 7b, red line) in concordance with the stability of the MPEF signal from the layer upon ablation at this wavelength (Figs. 5d, e). Fig. 7b also displays the LIF spectrum of a sample measured after complete removal of the dammar layer at 213 nm (blue line) with a band structure which is characteristic of the POPOP fluorophore [28] that has been exposed by ablation.

The Raman spectra of the samples confirm the above LIF results. An example is given in Fig. 8, which shows the case of the dammar surface before and after ablation with 150 ps pulses of 266 nm (black, continuous and red, dotted lines, respectively). Ablation at this wavelength results in an increased fluorescence background, in agreement with observations by MPEF and LIF measurements. As mentioned, the increased fluorescence is attributed to UV ablating laser light-induced oxidative degradation of dammar, i.e. C=C and C=O bond formation and creation of oxidation products [29, 31]. However, the characteristic dammar bands [29, 31], as indicated in the Figure 8, are not affected by ablation except for a slight intensity reduction [29].

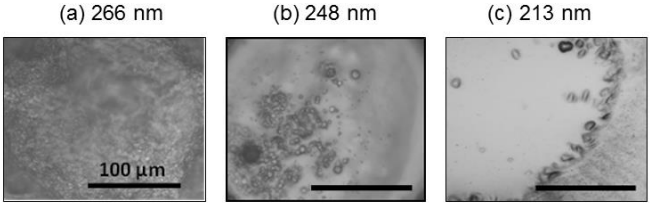

Fig. 6. Optical microscopy image of the dammar surface of bi-layer samples irradiated under the following conditions: (a) 266 nm, 176 pulses of 150 ps and F= 310 mJ/cm^2, (b) 248 nm, 300 pulses of 500 fs and F= 310 mJ/cm^2, and (c) 213 nm, 45 pulses of 150 ps and F= 120 mJ/cm^2. The length of the bar is 100 µm in all images.

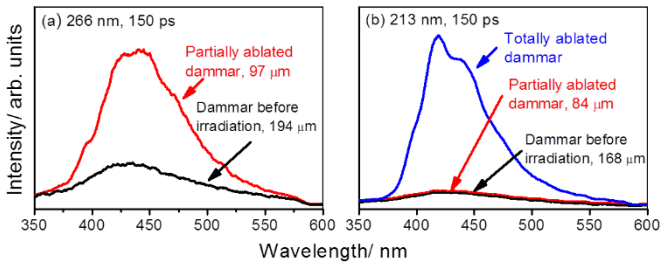

Fig. 7. Laser induced fluorescence (upon excitation at 248 nm) of the upper surface of the bi-layer samples before and after partial or total removal of the dammar layer by ablation with 150 ps pulses at (a) 266 nm and (b) 213 nm. The thickness of the varnish layer in each case is indicated.

4. Conclusions

In this work, the structural and in-depth photochemical modifications induced during ultraviolet laser removal of a dammar varnish coating on a photosensitive substrate, mimicking a paint layer, were assessed with micrometric resolution via nonlinear microscopy (NLM) imaging. According to the results obtained at the three different ablation wavelengths of this study (266, 248 and 213 nm), changes upon laser ablation of the Multi-Photon Excited Fluorescence signals finger post photochemical modifications of the varnish or of the photosensitive under-layer, while Third Harmonic Generation measurements indicate the presence of layer boundaries and, therefore, the reduction by laser ablation of the thickness of the varnish coating. The NLM measurements undoubtedly show that the absorption coefficient of the varnish at the ablation wavelength plays a more crucial role over the effects observed than the pulse duration (for pulses of 8, 15 ns, 150 ps and 500 fs), and that increased UV light absorption by dammar reduces the extent and the in-depth dimension of the photochemical modifications induced in the sample layers. In that respect, the

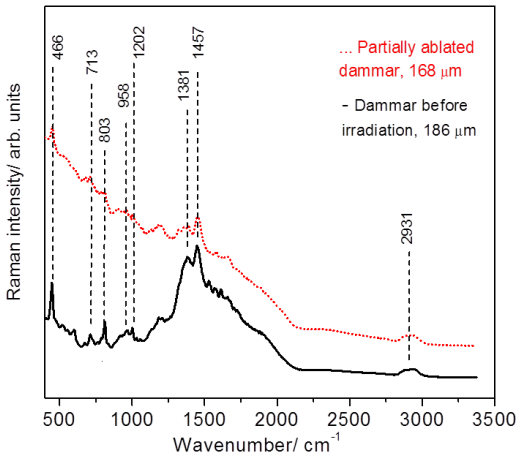

Fig. 8. Raman spectra of the dammar surface of a bi-layer sample before laser irradiation (black, continuous line) and following irradiation with 150 ps pulses at 266 nm red, dotted line). The thicknesses of the dammar layer before and after ablation are indicated. The dashed vertical lines identify characteristic dammar bands with wavenumbers in cm^{-1} [29, 31].

present NLM study clearly place evidence of the advantages of using an ablation wavelength that is strongly absorbed by the varnish. The present investigation was performed in dry, unaged samples. Although a nonlinear microscopy study of aged samples is to be completed, it is known that ageing improves the UV light absorbance of the varnish and therefore reduced photochemical changes should be expected.

Second and Third Harmonic Generation modalities can be implemented by easily upgrading a common multiphoton microscope, adding further capabilities for painting investigations. Although additional experimental results on more realistic painting substrates and on real substrates will follow this work, we can conclude that the results obtained herein are of direct application to laser cleaning of paintings and that nonlinear imaging microscopy methods can be extensively used as reliable, minimally invasive, high resolution assessment tools for the in situ monitoring of superficial and in depth structural and photochemical modifications induced upon laser cleaning of paintings based in the laser ablation removal of deteriorated varnish layers.

Acknowledgements

Funding has been provided by EU Horizon 2020 programs LASERLAB-EUROPE (H2020-INFRAIA-2014-2015, nº 654148) and IPERION-CH (H2020-INFRAIA-2014-2015, nº 654028), by Ministerio de Economía, Industria y Competitividad (MINECO) of Spain under Projects CTQ2013-43086-P and CTQ2016-75880-P and by program Geomateriales 2 (S2013/MIT-2914). M.O. thanks CSIC for a contract. We are grateful to D. Anglos (IESL-FORTH) for useful discussions.

References

1 E.R. De La Rie, *Anal. Chem.*, 1989, **61**, 1228A.
2 Knut Nicolaus, The Restoration of Paintings. Buckle's Books (Cambridge, United Kingdom) 1999.
3 P. Pouli, A. Selimis, S. Georgiou and C. Fotakis, *Acc. Chem. Res.*, 2010, **43**, 771.
4 M. Oujja, A. García, C. Romero, J.R. Vázquez de Aldana, P. Moreno and M. Castillejo, *Phys. Chem. Chem. Phys.*, 2011, **13**, 4625.
5 P. Pouli, M. Oujja and M. Castillejo, *Appl. Phys. A.,* 2012, **106**, 447.
6 M. Castillejo, M. Martín, M. Oujja, D. Silva, R. Torres, A. Manousaki and H. Gouveia, *Anal. Chem.,* 2002, **74**, 4662.
7 R. Teule, H. Scholten, O. van den Brink, R. Heeren, V. Zafiropulos, R. Hesterman, M. Castillejo, M. Martin, U. Ullenius, I. Larsson, F. Guerra-Librero, A. Silva, H. Gouveia and M. Albuquerque, *J. Cult. Herit.,* 2003, **4**, 257.
8 P. Bracco, G. Lanterna, M. Matteini, K. Nakahara, O. Sartiani, A. de Cruz, M.L. Wolbarsht, E. Adamkiewicz and M.P. Colombini, *J. Cult. Heritage*, 2003, **4,** 202s.
9 S. Gaspard, M. Oujja, P. Moreno, C. Méndez, A. García, C. Domingo and M. Castillejo, *Appl. Surf. Sci.,* 2008, **255,** 2675.
10 M. Oujja, P. Pouli, C. Domingo, C. Fotakis and M. Castillejo, *Appl. Spectrosc.*, 2010, **64**, 528.
11 S. Siano, J. Agresti, I. Cacciari, D. Ciofini, M. Mascalchi, I. Osticioli, A.A. Mencaglia, *Appl. Phys. A*, 2012, **106**, 419.
12 M. Oujja, M. Sanz, E. Rebollar, J.F. Marco, C. Domingo, P. Pouli, S. Kogou, C. Fotakis and M. Castillejo, *Spectrochim. Acta A*, 2013, **102,** 7.
13 P. Pouli, I.-A. Paun, G. Bounos, S. Georgiou and C. Fotakis, *Appl. Surf. Sci.*, 2008, **254**, 6875.
14 M. Lassithiotaki, A. Athanassiou, D. Anglos, S. Georgiou and C. Fotakis, *Appl. Phys. A*, 1999, **69**, 363.
15 A. Athanassiou, E. Andreou, A. Bonarou, V. Tornari, D. Anglos, S. Georgiou and C. Fotakis, *Appl. Surf. Sci.*, 2002, **197**, 757.
16 S. Georgiou, D. Anglos and C. Fotakis, *Contemporary Physics*, 2008, **49**, 1.
17 W.R. Zipfel, R.M. Williams and W.W. Webb, *Nat. Biotechnol.*, 2003, **21**, 1369.
18 A.M. Streets, A. Li, T. Chen and Y. Huang, *Anal. Chem.*, 2014, **86**, 8506.
19 E.J. Gualda, G. Filippidis, K. Melessanaki and C. Fotakis, *Appl. Spectrosc.*, 2009, **63**, 280.
20 A. Nevin, D. Comelli, I. Osticioli, G. Filippidis, K. Melessanaki, G. Valentini, R. Cubeddu and C. Fotakis, *Appl. Phys. A*, 2010, **100**, 599.
21 G. Filippidis, M. Massaouti, A. Selimis, E.J. Gualda, J.M. Manceau and S. Tzortzakis, *Appl. Phys. A*, 2011, **106**, 257.
22 G. Latour, J.-P. Echard, M. Didier and M.-C. Schanne-Klein, *Opt. Express*, 2012, **20**, 24623.
23 G. Filippidis, G.J. Tserevelakis, A. Selimis and C. Fotakis, *Appl. Phys. A*, 2015, **118**, 417.
24 T.E. Villafana, J.K. Delaney, W.S. Warren and M.C. Fischer, *J. Cult. Herit.*, 2016, **20**, 583.
25 P. Vounisiou, A. Selimis, G.J. Tserevelaki, K. Melessanaki, P. Pouli, G. Filippidis, C. Beltsios, S. Georgiou and C. Fotakis, *Appl. Phys. A*, 2010, **100**, 647.
26 G. Filippidis, M. Mari, L. Kelegkouri, A. Philippidis, A. Selimis, K. Melessanaki, M. Sygletou and C. Fotakis, *Microsc. Microanal.*, 2015, **21**, 510.
27 E. Rebollar, G. Bounos, M. Oujja, C. Domingo, S. Georgiou and M. Castillejo, *J. Phys. Chem.*, B 2006, **110**, 14215.
28 S.A. El-Daly, S.A. El-Azim, F.M. Elmekawey, B.Y. Elbaradei, S.A. Shama and A.M. Asiri, *International Journal of Photoenergy*, 2012, Article ID 458126, doi:10.1155/2012/458126.
29 D. Ciofini M. Oujja, M. V. Cañamares, S. Siano and M. Castillejo*, Microchemical J.*, 2016, **124**, 792.
30 G.W. White, *Microscope*, 1970, **18**, 51.
31 A. Nevin, D. Comelli, I. Osticioli, L. Toniolo, G. Valentini and R. Cubeddu, *Anal. Bioanal. Chem.*, 2009, **395**, 2139.
32 "Photobleaching", A. Diaspro, G. Chirico, C. Usai, P. Ramoino and J. Dobrucki, Handbook of Biological Confocal Microscopy, Third Edition, edited by James B. Pawley, Springer Science+Business Media, LLC, New York, 2006.